

Search for $B_s^0 \rightarrow \eta' X_{s\bar{s}}$ at Belle Using a Semi-Inclusive Method

S. Dubey, T. E. Browder, M. Bessner, M. T. Hedges, A. Natochii, K. Nishimura, S. E. Vahsen, and G. Varner
University of Hawaii, Honolulu, Hawaii 96822

H. Aihara, Y. Jin, and Y. Onuki
Department of Physics, University of Tokyo, Tokyo 113-0033

S. Al Said
*Department of Physics, Faculty of Science, University of Tabuk, Tabuk 71451 and
Department of Physics, Faculty of Science, King Abdulaziz University, Jeddah 21589*

D. M. Asner and N. K. Nisar
Brookhaven National Laboratory, Upton, New York 11973

T. Aushev
Higher School of Economics (HSE), Moscow 101000

R. Ayad
Department of Physics, Faculty of Science, University of Tabuk, Tabuk 71451

V. Babu, S. Cunliffe, T. Ferber, A. Rostomyan, F. Tenchini, and H. Ye
Deutsches Elektronen-Synchrotron, 22607 Hamburg

S. Bahinipati
Indian Institute of Technology Bhubaneswar, Satya Nagar 751007

P. Behera, J. Libby, and N. Rout
Indian Institute of Technology Madras, Chennai 600036

J. Bennett and R. Kroeger
University of Mississippi, University, Mississippi 38677

B. Bhuyan
Indian Institute of Technology Guwahati, Assam 781039

S. Bilokin and T. Kuhr
Ludwig Maximilians University, 80539 Munich

J. Biswal, R. Pestotnik, and M. Starič
J. Stefan Institute, 1000 Ljubljana

A. Bobrov, D. Epifanov, N. Gabyshev, A. Garmash, K. Gudkova, P. Krokovny, B. Shwartz, Y. Usov, and V. Zhilich
*Budker Institute of Nuclear Physics SB RAS, Novosibirsk 630090 and
Novosibirsk State University, Novosibirsk 630090*

G. Bonvicini, D. Cinabro, and K. Kumara
Wayne State University, Detroit, Michigan 48202

A. Bozek
H. Niewodniczanski Institute of Nuclear Physics, Krakow 31-342

M. Bračko and S. Korpar
*University of Maribor, 2000 Maribor and
J. Stefan Institute, 1000 Ljubljana*

M. Campajola, F. Di Capua, and M. Merola
INFN - Sezione di Napoli, 80126 Napoli and

Università di Napoli Federico II, 80126 Napoli

D. Červenkov and Z. Doležal
Faculty of Mathematics and Physics, Charles University, 121 16 Prague

B. G. Cheon, H. E. Cho, C. H. Kim, and Y. Unno
Department of Physics and Institute of Natural Sciences, Hanyang University, Seoul 04763

K. Chilikin, P. Oskin, E. Solovieva, and V. Zhukova
P.N. Lebedev Physical Institute of the Russian Academy of Sciences, Moscow 119991

K. Cho
Korea Institute of Science and Technology Information, Daejeon 34141

Y. Choi
Sungkyunkwan University, Suwon 16419

S. Choudhury, R. Dhamija, A. Giri, L. Nayak, and S. Sandilya
Indian Institute of Technology Hyderabad, Telangana 502285

S. Das, K. Lalwani, and C. Sharma
Malaviya National Institute of Technology Jaipur, Jaipur 302017

D. Dossett, C. MacQueen, and M. E. Sevier
School of Physics, University of Melbourne, Victoria 3010

S. Eidelman
*Budker Institute of Nuclear Physics SB RAS, Novosibirsk 630090
 Novosibirsk State University, Novosibirsk 630090 and
 P.N. Lebedev Physical Institute of the Russian Academy of Sciences, Moscow 119991*

B. G. Fulsom, C. Hadjivasiliou, and J. F. Strube
Pacific Northwest National Laboratory, Richland, Washington 99352

R. Garg
Panjab University, Chandigarh 160014

V. Gaur, T. D. Kimmel, L. E. Piiilonen, and Z. S. Stottler
Virginia Polytechnic Institute and State University, Blacksburg, Virginia 24061

P. Goldenzweig, F. Metzner, and M. T. Prim
Institut für Experimentelle Teilchenphysik, Karlsruher Institut für Technologie, 76131 Karlsruhe

B. Golob, P. Križan, T. Podobnik, and L. Santelj
*Faculty of Mathematics and Physics, University of Ljubljana, 1000 Ljubljana and
 J. Stefan Institute, 1000 Ljubljana*

D. Greenwald
Department of Physics, Technische Universität München, 85748 Garching

Y. Guan, K. Kinoshita, L. K. Li, and A. Sangal
University of Cincinnati, Cincinnati, Ohio 45221

K. Hayasaka, Y. Seino, and M. Watanabe
Niigata University, Niigata 950-2181

H. Hayashii and K. Miyabayashi
Nara Women's University, Nara 630-8506

W.-S. Hou and J.-G. Shiu
Department of Physics, National Taiwan University, Taipei 10617

C.-L. Hsu and B. D. Yabsley
School of Physics, University of Sydney, New South Wales 2006

K. Inami
Graduate School of Science, Nagoya University, Nagoya 464-8602

A. Ishikawa, R. Itoh, M. Nakao, S. Nishida, Y. Sakai, K. Sumisawa, S. Uno, and Y. Ushiroda
*High Energy Accelerator Research Organization (KEK), Tsukuba 305-0801 and
 SOKENDAI (The Graduate University for Advanced Studies), Hayama 240-0193*

M. Iwasaki
Osaka City University, Osaka 558-8585

Y. Iwasaki and H. Kichimi
High Energy Accelerator Research Organization (KEK), Tsukuba 305-0801

E.-J. Jang
Gyeongsang National University, Jinju 52828

C. W. Joo
Kavli Institute for the Physics and Mathematics of the Universe (WPI), University of Tokyo, Kashiwa 277-8583

K. K. Joo
Chonnam National University, Gwangju 61186

A. B. Kaliyar, G. B. Mohanty, and D. Sahoo
Tata Institute of Fundamental Research, Mumbai 400005

T. Kawasaki
Kitasato University, Sagamihara 252-0373

D. Y. Kim
Soongsil University, Seoul 06978

S. H. Kim and T. J. Moon
Seoul National University, Seoul 08826

Y.-K. Kim, Y.-J. Kwon, and S.-H. Park
Yonsei University, Seoul 03722

R. Kulasiri
Kennesaw State University, Kennesaw, Georgia 30144

R. Kumar
Punjab Agricultural University, Ludhiana 141004

J. S. Lange
Justus-Liebig-Universität Gießen, 35392 Gießen

S. C. Lee and J. Li
Kyungpook National University, Daegu 41566

C. H. Li
Liaoning Normal University, Dalian 116029

Y. B. Li

Peking University, Beijing 100871

L. Li Gioi

Max-Planck-Institut für Physik, 80805 München

D. Liventsev

*Wayne State University, Detroit, Michigan 48202 and
High Energy Accelerator Research Organization (KEK), Tsukuba 305-0801*

M. Masuda

*Earthquake Research Institute, University of Tokyo, Tokyo 113-0032 and
Research Center for Nuclear Physics, Osaka University, Osaka 567-0047*

T. Matsuda

University of Miyazaki, Miyazaki 889-2192

R. Mizuk

*P.N. Lebedev Physical Institute of the Russian Academy of Sciences, Moscow 119991 and
Higher School of Economics (HSE), Moscow 101000*

S. Mohanty

*Tata Institute of Fundamental Research, Mumbai 400005 and
Utkal University, Bhubaneswar 751004*

M. Nayak

School of Physics and Astronomy, Tel Aviv University, Tel Aviv 69978

S. Ogawa

Toho University, Funabashi 274-8510

H. Ono

*Nippon Dental University, Niigata 951-8580 and
Niigata University, Niigata 950-2181*

G. Pakhlova

*Higher School of Economics (HSE), Moscow 101000 and
P.N. Lebedev Physical Institute of the Russian Academy of Sciences, Moscow 119991*

S. Pardi

INFN - Sezione di Napoli, 80126 Napoli

T. K. Pedlar

Luther College, Decorah, Iowa 52101

E. Prencipe

Forschungszentrum Jülich, 52425 Jülich

G. Russo

Università di Napoli Federico II, 80126 Napoli

T. Sanuki

Department of Physics, Tohoku University, Sendai 980-8578

V. Savinov and E. Wang

University of Pittsburgh, Pittsburgh, Pennsylvania 15260

G. Schnell

University of the Basque Country UPV/EHU, 48080 Bilbao and

IKERBASQUE, Basque Foundation for Science, 48013 Bilbao

C. Schwanda

Institute of High Energy Physics, Vienna 1050

K. Senyo

Yamagata University, Yamagata 990-8560

M. Shapkin

Institute for High Energy Physics, Protvino 142281

M. Takizawa

Showa Pharmaceutical University, Tokyo 194-8543

*J-PARC Branch, KEK Theory Center, High Energy Accelerator Research Organization (KEK), Tsukuba 305-0801 and
Meson Science Laboratory, Cluster for Pioneering Research, RIKEN, Saitama 351-0198*

U. Tamponi

INFN - Sezione di Torino, 10125 Torino

K. Tanida

Advanced Science Research Center, Japan Atomic Energy Agency, Naka 319-1195

Y. Tao

University of Florida, Gainesville, Florida 32611

K. Trabelsi and S. Watanuki

Université Paris-Saclay, CNRS/IN2P3, IJCLab, 91405 Orsay

M. Uchida

Tokyo Institute of Technology, Tokyo 152-8550

R. Van Tonder

University of Bonn, 53115 Bonn

C. H. Wang

National United University, Miao Li 36003

P. Wang

Institute of High Energy Physics, Chinese Academy of Sciences, Beijing 100049

X. Xu

Soochow University, Suzhou 215006

W. Yan and Z. P. Zhang

*Department of Modern Physics and State Key Laboratory of Particle Detection and Electronics,
University of Science and Technology of China, Hefei 230026*

S. B. Yang and J. H. Yin

Korea University, Seoul 02841

(The Belle Collaboration)

(Dated: March 1, 2025)

We report the first search for the penguin-dominated process $B_s^0 \rightarrow \eta' X_{s\bar{s}}$ using a semi-inclusive method. A 121.4 fb^{-1} integrated luminosity $\Upsilon(5S)$ data set collected by the Belle experiment, at the KEKB asymmetric-energy e^+e^- collider, is used. We observe no statistically significant signal and including all uncertainties, we set a 90% confidence level upper limit on the partial branching fraction at 1.4×10^{-3} for $M(X_{s\bar{s}}) \leq 2.4 \text{ GeV}/c^2$.

The study of the decay of B mesons — bound states of a b antiquark and either a u , d , s , or c quark — has been fruitful for the interrogation of rare processes, elucidating the strong and weak interactions of the Standard Model (SM) of particle physics. According to the SM flavor-changing neutral currents are forbidden in B decays at leading-order, but may effectively occur at higher-order in so-called “penguin” processes [1].

The CLEO collaboration measured a larger than expected branching fraction (BF) for the charmless decay (decays whose primary decay products lack a charm quark) $B \rightarrow \eta' X_s$ as $\mathcal{B}(B \rightarrow \eta' X_s) = [4.6 \pm 1.1 \text{ (stat.)} \pm 0.4 \text{ (syst.)} \pm 0.5 \text{ (bkg.)}] \times 10^{-4}$, with $M(X_s) < 2.35 \text{ GeV}/c^2$, where the third uncertainty is due to the background subtraction [2, 3]. BaBar measured $\mathcal{B}(B \rightarrow \eta' X_s) = [3.9 \pm 0.8 \text{ (stat.)} \pm 0.5 \text{ (syst.)} \pm 0.8 \text{ (model)}] \times 10^{-4}$, for the same $M(X_s)$ requirement [4]. Belle previously measured the BF for the related process $B \rightarrow \eta X_s$ as $\mathcal{B}(B \rightarrow \eta X_s) = [26.1 \pm 3.0 \text{ (stat.)}^{+1.9}_{-2.1} \text{ (syst.)}^{+4.0}_{-7.1} \text{ (model)}] \times 10^{-5}$ [5]. While the η' meson itself is interesting [6] as its mass is higher than is expected from symmetry considerations, it is the unexpected BF enhancement seen in these measurements that has generated considerable interest. In Ref. [7], for example, the predicted BF for $B \rightarrow \eta' X$ is 1.3×10^{-4} . Explanations for this apparent enhancement focus on processes such as the $b \rightarrow sg$ transition, which is modified to an anomalous $b \rightarrow sg^*$ process, where $g^* \rightarrow g\eta'$, with the gluon coupling to the η' singlet [8–14]. Hence, glueball coupling may provide an explanation for these decays involving the η' .

Inclusive $b \rightarrow sg$ processes have not yet been investigated using the B_s^0 meson. In this letter we report the first search for the decay $B_s^0 \rightarrow \eta' X_{s\bar{s}}$ using a semi-inclusive method [15] with data collected at the $\Upsilon(5S)$ resonance by the Belle detector at the KEKB asymmetric-energy e^+e^- collider in Japan [16].

To lowest order, the amplitude for $B_s^0 \rightarrow \eta' X_{s\bar{s}}$ contains contributions from QCD penguin diagrams, the anomalous $g\eta'$ coupling, the tree-level color-suppressed $b \rightarrow u$ diagram, and the $b \rightarrow s(\gamma, Z)$ electroweak penguin diagrams, shown in Fig. 1 [17].

The Belle detector is a large-solid-angle magnetic spectrometer that consists of a silicon vertex detector (SVD), a 50-layer central drift chamber (CDC), an array of aerogel threshold Cherenkov counters (ACC), a barrel-like arrangement of time-of-flight scintillation counters (TOF), and an electromagnetic calorimeter comprised of CsI(Tl) crystals (ECL) located inside a superconducting solenoid coil that provides a 1.5 T magnetic field. An iron flux-return located outside of the coil is instrumented to detect K_L^0 mesons and to identify muons. The $\Upsilon(5S)$ data sample used a 1.5 cm radius beampipe, a 4-layer SVD,

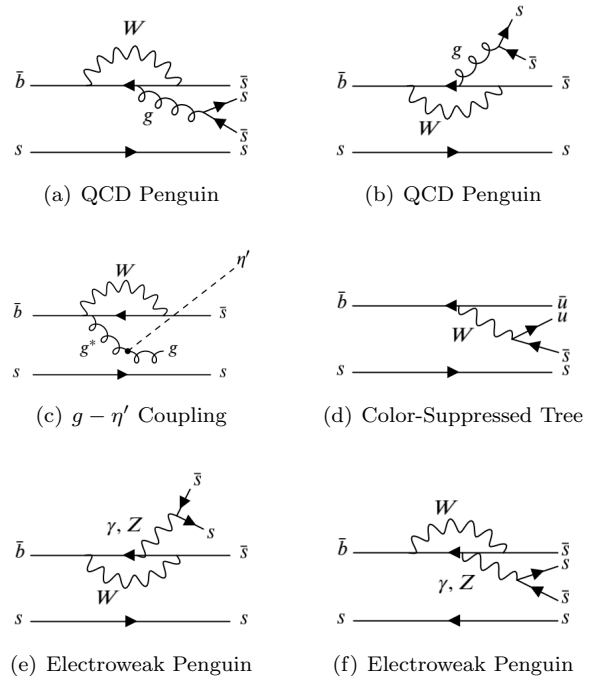


FIG. 1. Lowest-order diagrams contributing to $B_s^0 \rightarrow \eta' X_{s\bar{s}}$

and a small-inner-cell CDC [18].

We use the 121.4 fb^{-1} data sample recorded by Belle, taken at the center-of-mass (CM) energy $\sqrt{s} = 10.866 \text{ GeV}$. This corresponds to $(7.11 \pm 1.30) \times 10^6 B_s^0 \bar{B}_s^0$ pairs, the world’s largest $\Upsilon(5S)$ sample in e^+e^- collisions [19]. A blind analysis is performed, whereby the selection criteria are first optimized on Monte Carlo (MC) simulations before being applied to the data. A signal MC sample for $B_s^0 \rightarrow \eta' X_{s\bar{s}}$ is generated using EvtGen [20] and the detector response is simulated using GEANT3 [21], with PHOTOS describing final-state radiation [22]. The MC-generated mass of the $X_{s\bar{s}}$ system is bounded below by the two-(charged) kaon mass $0.987 \text{ GeV}/c^2$ and has an upper bound of $3.0 \text{ GeV}/c^2$. The $X_{s\bar{s}}$ mass is generated as a flat distribution and is fragmented by PYTHIA 6 [23].

The B_s^0 ($\bar{b}s$) and \bar{B}_s^0 ($b\bar{s}$) candidates are reconstructed using a semi-inclusive method in which the $X_{s\bar{s}}$ is reconstructed as a system of two kaons, either K^+K^- or $K^\pm K_S^0$ ($\rightarrow \pi^+\pi^-$), and up to four pions with at most one π^0 , where the π^0 decays via the channel $\pi^0 \rightarrow \gamma\gamma$. The η' is reconstructed in the channel $\eta' \rightarrow \eta(\rightarrow \gamma\gamma)\pi^+\pi^-$. The experimental signature is divided into two classes of decay modes: without ($B_s^0 \rightarrow \eta' K^+K^- + n\pi$) and with ($B_s^0 \rightarrow \eta' K^\pm K_S^0 + n\pi$) a K_S^0 . These classes are analyzed

separately, with the weighted average BFs taken at the end. Charge-conjugate decays are included unless explicitly stated otherwise.

Well-constrained charged tracks are required to have a transverse momentum p_T greater than 50 MeV/ c . Separation of the charged kaons and charged pions is provided by the CDC [24], ACC [25], and the TOF [26] systems. Information from these subdetectors is combined to form a likelihood ratio for the charged kaon hypothesis: $P_{K^\pm} = L_{K^\pm}/(L_{K^\pm} + L_{\pi^\pm})$. For this analysis, the selections $P_{K^\pm} > 0.6$ for K^\pm and $P_{K^\pm} < 0.6$ for π^\pm are applied. The efficiency to correctly identify a pion (kaon) is 98% (88)%, with a misidentification rate of 4% (12)% [5].

The π^0 candidate mass range is $M(\gamma\gamma) \in [0.089, 0.180]$ GeV/ c^2 ($\pm 5\sigma$ window). The π^0 candidates are kinematically constrained to the nominal mass [27]. In the ECL, the photons constituting the π^0 are required to have energies greater than 50 MeV in the barrel region, greater than 100 MeV in the endcaps, and the ratio of their energy depositions in a 3×3 ECL crystal array to that in a 5×5 crystal array around the central crystal, is required to be greater than 0.9. To further reduce combinatorial background, a requirement on the π^0 laboratory-frame momentum to be greater than 0.2 GeV/ c is imposed.

The η is reconstructed in a two-photon asymmetric invariant mass window $M_\eta \in [0.476, 0.617]$ GeV/ c^2 ($5.3\sigma_L$, $10\sigma_R$). The asymmetry is due to energy leakage in the ECL, causing the η mass distribution to be asymmetric. Each photon is required to have $E_\gamma > 0.1$ GeV. A requirement on the photon-energy asymmetry ratio $|E_{\gamma 1} - E_{\gamma 2}|/(E_{\gamma 1} + E_{\gamma 2}) < 0.6$ is applied to further suppress the background. The η' mesons are reconstructed in a fully efficient mass window $M_{\eta'} \in [0.933, 0.982]$ GeV/ c^2 ($\pm 10\sigma$). The η and η' masses are kinematically fit to the world average [27]. The mass range of the K_S^0 is $M_{K_S^0} \in [0.487, 0.508]$ GeV/ c^2 ($\pm 3\sigma$ window).

The $X_{s\bar{s}}$ system is reconstructed as a system of kaons and pions, which is in turn combined with the η' to form B_s candidates. Two variables important in extracting the signal are the energy difference ΔE , defined as $\Delta E = E_{B_s} - E_{\text{beam}}$ and the beam-energy-constrained mass, defined as $M_{\text{bc}} = \sqrt{E_{\text{beam}}^2/c^4 - p_{B_s}^2/c^2}$, where $E_{\text{beam}} = \sqrt{s}/2$, E_{B_s} is the energy of the B_s , and p_{B_s} is the magnitude of the B_s three-momentum in the CM frame.

An initial reduction in continuum background ($e^+e^- \rightarrow q\bar{q}$, $q = u, d, s, c$) is done with a selection on the ratio of the second to the zeroth order Fox-Wolfram moments $R_2 \leq 0.6$ [28]. A neural network (NN), NeuroBayes [29], is used to further suppress continuum background, with other backgrounds being reduced as well. The NN is trained to primarily discriminate between event topologies using event shape variables [30]. Signal events have a spherical topology, while continuum background events are jet-like. The NN is trained using these variables on independent signal and continuum background MC simulations. The NN output variable O_{NN} describes, effec-

tively, the probability that a B_s^0 candidate came from an event whose topology is spherical or jet-like.

To obtain a specific O_{NN} selection, the figure-of-merit (FOM) $S/\sqrt{S+B}$ is optimized as a function of O_{NN} , where S and B are the fitted signal and background yields from an MC sample that is passed through the trained network. This MC contains an approximately data-equivalent background and an enhanced signal. This was done assuming $\mathcal{B}(B_s^0 \rightarrow \eta' X_{s\bar{s}}) = 2 \times 10^{-4}$; this is 1.6 standard deviations below the BaBar central value for $B \rightarrow \eta' X_s$. The value of O_{NN} corresponding to the maximum value of the FOM is selected. Events having O_{NN} values below this selection are rejected. Separate optimizations are done for $B_s^0 \rightarrow \eta' K^+ K^- + n\pi$ and $B_s^0 \rightarrow \eta' K^\pm K_S^0 + n\pi$. The NN requirement reduces continuum background by more than 97% in both cases, while preserving 39% and 53% of signal events for $B_s^0 \rightarrow \eta' K^+ K^- + n\pi$ and $B_s^0 \rightarrow \eta' K^\pm K_S^0 + n\pi$, respectively. The two experimental signatures have different background levels and efficiencies, and hence their NNs are optimized separately.

After an initial requirement of $M_{\text{bc}} > 5.30$ GeV/ c^2 , $|\Delta E| < 0.35$ GeV, and $M(X_{s\bar{s}}) \leq 2.4$ GeV/ c^2 , and after all final selections are applied, there are an average of 6.4 candidates per event for $B_s^0 \rightarrow \eta' K^+ K^- + n\pi$ and 26.0 for $B_s^0 \rightarrow \eta' K^\pm K_S^0 + n\pi$. To select the best candidate per event, the candidate with the smallest χ^2 given by $\chi^2 = \chi_{\text{vtx}}^2/\text{ndf} + (\Delta E - \mu_{\Delta E})^2/\sigma_{\Delta E}^2$ is selected, where ΔE is calculated on a candidate-by-candidate basis, and $\mu_{\Delta E}$ is the mean energy difference obtained through studies of signal MC of individual exclusive $B_s^0 \rightarrow \eta' X_{s\bar{s}}$ decay modes. Here $\chi_{\text{vtx}}^2/\text{ndf}$ is the reduced χ^2 from a successful vertex fit of the primary charged daughter particles of the $X_{s\bar{s}}$. From signal MC, the efficiency of the best candidate selection is 85.5% for $B_s^0 \rightarrow \eta' K^+ K^- + n\pi$ and 43.2% for $B_s^0 \rightarrow \eta' K^\pm K_S^0 + n\pi$, in the signal region. The fraction of B_s^0 candidates passing best candidate selection that are correctly reconstructed is 94.0% for $B_s^0 \rightarrow \eta' K^+ K^- + n\pi$ and 60.4% for $B_s^0 \rightarrow \eta' K^\pm K_S^0 + n\pi$. These numbers are obtained after all final selections are applied.

Other backgrounds were studied as sources of potential peaking background. Due to the signal final state, it is difficult to have backgrounds that will be equivalent in topology and strangeness, and that are not highly suppressed. However, one such unmeasured mode is $B_s^0 \rightarrow \eta' D_s \pi$. Reconstruction efficiency is estimated using MC events and an expected number of peaking events is determined. For $B_s^0 \rightarrow \eta' D_s \pi$ the BF is assumed to be similar to $B^0 \rightarrow D^- \pi^+ \rho^0$, for which the world average is $[1.1 \pm 1.0] \times 10^{-3}$ [27]. After applying all final selections, the total number of expected peaking events is less than one. There is a negligible amount of peaking background based on studies of $B_{(s)}^0 \bar{B}_{(s)}^0$ MC samples.

The decay $B \rightarrow \eta' K^{0*}$ can contribute to peaking background if the pion from $K^{0*} \rightarrow K^- \pi^+$ is misidentified. The world average BF is $[2.8 \pm 0.6] \times 10^{-6}$ [27]. From this and the pion misidentification rate, we expect the background contribution from this mode to be negligi-

ble.

The color-suppressed, tree-level process $B_s^0 \rightarrow \bar{D}^0 \eta'$, with $D^0 \rightarrow K^+ K^-$ could potentially contribute to the peaking background. However, $B^0 \rightarrow \bar{D}^0 \eta'$ has a measured BF of $\mathcal{B}(B^0 \rightarrow \bar{D}^0 \eta') = [1.38 \pm 0.16] \times 10^{-4}$. The process $D^0 \rightarrow K^+ K^-$ is Cabibbo-suppressed and has a measured BF of $\mathcal{B}(D^0 \rightarrow K^+ K^-) = [4.08 \pm 0.06] \times 10^{-3}$ [27]. Assuming $SU(3)$ symmetry, we expect there to be less than one event from $B_s^0 \rightarrow \bar{D}^0 \eta'$, for this analysis.

For signal extraction, fitting is done in $0.2 \text{ GeV}/c^2$ bins of $X_{s\bar{s}}$ mass, up to $2.4 \text{ GeV}/c^2$, using unbinned maximum-likelihood fits. All submodes are combined for fitting. Signal extraction is done by fitting the M_{bc} distribution in the region $M_{bc} > 5.30 \text{ GeV}/c^2$, $-0.12 \leq \Delta E \leq 0.05 \text{ GeV}$.

The $\Upsilon(5S)$ decays to B_s^0 pairs with a fraction of 0.172 ± 0.030 [19] and of this fraction the $\Upsilon(5S)$ has three channels for the B_s^0 decays: $\Upsilon(5S) \rightarrow B_s^{0*} \bar{B}_s^{0*}$, $\Upsilon(5S) \rightarrow B_s^0 \bar{B}_s^{0*}$ and $B_s^{0*} \bar{B}_s^0$, and $\Upsilon(5S) \rightarrow B_s^0 \bar{B}_s^0$. The rates are 87.0%, 7.3%, and 5.7%, respectively [19]. The low-energy photon from $B_s^{0*} \rightarrow B_s^0 \gamma$ is not reconstructed. This has the effect of shifting the mean of the ΔE distribution to a value of approximately -50 MeV .

The signal is modeled as the sum of three Gaussian probability density functions (PDFs) that correspond to the three $\Upsilon(5S)$ decays described in the previous paragraph. For analysis of the $\Upsilon(5S)$ data, their shape parameters are empirically derived from a $B_s^0 \rightarrow D_s^- \rho^+$ data control sample. The means and widths of the signal Gaussians are fixed from this. The dominant non-peaking background is from continuum with others coming from generic $B_s^{0(*)} \bar{B}_s^{0(*)}$ and $B\bar{B}X$ decays. The non-peaking background fit component is an ARGUS PDF [31] with a fixed shape parameter, determined from fits to $\Upsilon(5S)$ data NN sidebands. The ARGUS endpoint is fixed at $5.434 \text{ GeV}/c^2$, the kinematic limit of M_{bc} . The full model is the sum of the signal and background PDFs, with the signal and background yields allowed to float.

The signal reconstruction efficiency, defined as $\epsilon_i = N_i^{\text{rec}}/N_i^{\text{gen}}$, is determined from fitting signal MC sample, in each $X_{s\bar{s}}$ mass bin i after all selections are applied. Here, $N_i^{\text{gen}} = N_i^{B_s^0 \rightarrow \eta' K^+ K^- + n\pi} + N_i^{B_s^0 \rightarrow \eta' K^\pm K_S^0 + n\pi} + N_i^{\text{other}}$, is the number of generated B_s^0 mesons in the signal MC sample. The quantity N_i^{other} is the number of generated B_s^0 mesons that do not belong to either of the two classes of signal modes: $B_s^0 \rightarrow \eta' K^+ K^- + n\pi$ and $B_s^0 \rightarrow \eta' K^\pm K_S^0 + n\pi$ [32]. The quantity N_i^{rec} is the number of events found from the Gaussian signal fit in the i -th $X_{s\bar{s}}$ mass bin.

The BF is calculated as $\mathcal{B}(B_s^0 \rightarrow \eta' X_{s\bar{s}})_i = N_i^{\text{sig}} / (2 \times N_{B_s^{0(*)} \bar{B}_s^{0(*)}} \epsilon'_i [\mathcal{B}(\eta \rightarrow \gamma\gamma) \mathcal{B}(\eta' \rightarrow \pi^+ \pi^- \eta)])$, where i denotes the mass bins of $X_{s\bar{s}}$, the ϵ'_i are the bin-by-bin MC signal reconstruction efficiencies ϵ_i , corrected for data-MC discrepancies in NN selection, best candidate selection, particle identification, tracking efficiency, $\eta \rightarrow \gamma\gamma$ reconstruction, $\pi^0 \rightarrow \gamma\gamma$ reconstruction, and $K_S^0 \rightarrow \pi^+ \pi^-$ reconstruction. The quantity N_i^{sig} is the number

of fitted signal events and the quantity $N_{B_s^{0(*)} \bar{B}_s^{0(*)}}$ is the number of produced $B_s^{0(*)} \bar{B}_s^{0(*)}$ pairs.

Figures 2 and 3 show the sum of the fits, whose results are listed in Tables I and II, respectively, overlaid on the data. The central value for $\mathcal{B}(B_s^0 \rightarrow \eta' X_{s\bar{s}})$ is estimated by taking the weighted average of the total BF central values for $B_s^0 \rightarrow \eta' K^+ K^- + n\pi$ and $B_s^0 \rightarrow \eta' K^\pm K^0 + n\pi$. These are obtained by summing the BFs listed in Tables I and II, for $B_s^0 \rightarrow \eta' K^+ K^- + n\pi$ and $B_s^0 \rightarrow \eta' K^\pm K^0 + n\pi$, respectively. The weights for the average central value are obtained from the statistical uncertainties. Systematic uncertainties are added in quadrature; fragmentation model (FM) uncertainties are added linearly within a class and for the final weighted average, these class sums are added in quadrature.

The statistical significance in each $X_{s\bar{s}}$ mass bin is calculated as $\mathcal{S} = \sqrt{-2 \ln(\mathcal{L}_0/\mathcal{L}_{\text{max}})}$, where \mathcal{L}_0 is the likelihood at zero signal yield and \mathcal{L}_{max} is the maximum likelihood. No statistically significant excess of events is observed in any $X_{s\bar{s}}$ mass bin. We set an upper limit on the partial BF (a BF with the requirement $M(X_{s\bar{s}}) \leq 2.4 \text{ GeV}/c^2$) at 90% confidence level by integrating a Gaussian likelihood function whose standard deviation is estimated by the sum in quadrature of the positive statistical and systematic uncertainties [33]. The standard deviation, σ , is approximately 8.6×10^{-4} . The integral is restricted to the physically allowed region above zero, giving an upper limit on $\mathcal{B}(B_s^0 \rightarrow \eta' X_{s\bar{s}})$. As a result, 1.68σ is added to the weighted average central value to obtain the 90% confidence level upper limit.

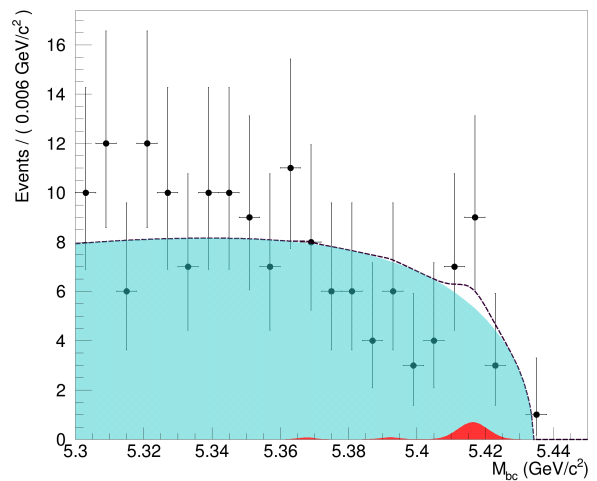


FIG. 2. Sum of the fits to all $M(X_{s\bar{s}})$ bins overlaid on the M_{bc} distribution, for the decay $B_s^0 \rightarrow \eta' (\rightarrow \eta \pi^+ \pi^-) X_{s\bar{s}}$ for $B_s^0 \rightarrow \eta' K^+ K^- + n\pi$ submodes and $M(X_{s\bar{s}}) \leq 2.4 \text{ GeV}/c^2$ and with all selections applied. The light blue shaded region is the sum of the background fits, the red shaded region is the sum of the signal fits, and the black dashed curve is the sum of the two.

The central value of the BF is $\mathcal{B}(B_s^0 \rightarrow \eta' X_{s\bar{s}}) = [-0.7$

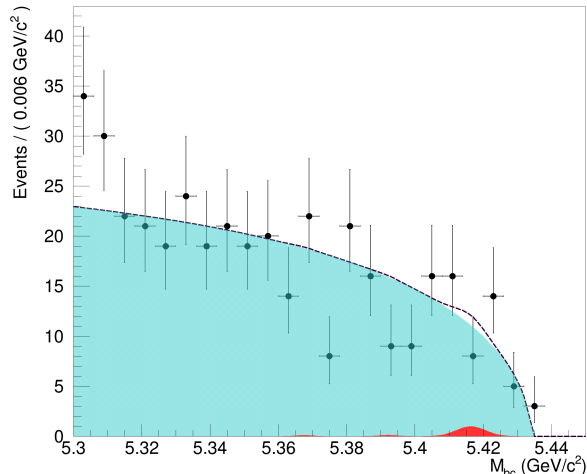


FIG. 3. Sum of the fits to all $M(X_{s\bar{s}})$ bins overlaid on the M_{bc} distribution, for the decay $B_s^0 \rightarrow \eta'(\rightarrow \eta\pi^+\pi^-)X_{s\bar{s}}$ for $B_s^0 \rightarrow \eta'K^\pm K_S^0 + n\pi$ submodes and $M(X_{s\bar{s}}) \leq 2.4 \text{ GeV}/c^2$ and with all selections applied. The light blue shaded region is the sum of the background fits, the red shaded region is the sum of the signal fits, and the black dashed curve is the sum of the two.

TABLE I. Results for the $B_s^0 \rightarrow \eta'K^+K^- + n\pi$ submodes, from the $121.4 \text{ fb}^{-1} \Upsilon(5S)$ data set; the table contains the $M(X_{s\bar{s}})$ bin in units of GeV/c^2 , corrected reconstruction efficiency (ϵ'), number of fitted signal events N_{sig} , and \mathcal{B} , the central value of the partial BF.

$M(X_{s\bar{s}})$	$\epsilon'(\%)$	N_{sig}	$\mathcal{B}(B_s^0 \rightarrow \eta'X_{s\bar{s}}) (10^{-4})$
1.0 - 1.2	3.6 ± 0.08	$0.4^{+2.6}_{-1.9}$	$0.05^{+0.30}_{-0.22} \text{ (stat.) } ^{+0.004}_{-0.005} \text{ (syst.)}$
1.2 - 1.4	2.8 ± 0.08	$0.08^{+2.4}_{-1.7}$	$0.01^{+0.36}_{-0.28} \text{ (stat.) } ^{+0.001}_{-0.001} \text{ (syst.)}$
1.4 - 1.6	0.9 ± 0.04	$0.7^{+2.5}_{-1.8}$	$0.3^{+1.1}_{-0.8} \text{ (stat.) } ^{+0.04}_{-0.04} \text{ (syst.)}$
1.6 - 1.8	0.5 ± 0.03	$0.4^{+2.1}_{-1.4}$	$0.3^{+1.6}_{-1.1} \text{ (stat.) } ^{+0.05}_{-0.1} \text{ (syst.)}$
1.8 - 2.0	0.3 ± 0.03	$1.4^{+2.6}_{-2.0}$	$1.7^{+3.3}_{-2.5} \text{ (stat.) } ^{+0.4}_{-0.6} \text{ (syst.)}$
2.0 - 2.2	0.2 ± 0.02	$0.3^{+3.7}_{-3.4}$	$0.6^{+7.1}_{-6.4} \text{ (stat.) } ^{+0.2}_{-0.2} \text{ (syst.)}$
2.2 - 2.4	0.1 ± 0.02	$-2.3^{+3.8}_{-3.4}$	$-7.0^{+11.6}_{-10.4} \text{ (stat.) } ^{+1.7}_{-4.1} \text{ (syst.)}$

$\pm 8.1 \text{ (stat.)} \pm 0.7 \text{ (syst.) } ^{+3.0}_{-6.0} \text{ (FM)} \pm 0.1 (N_{B_s^{0(*)}\bar{B}_s^{0(*)}}) \times 10^{-4}$. The FM uncertainty is obtained by considering alternate sets of $X_{s\bar{s}}$ fragmentation parameter values in PYTHIA and redetermining the signal reconstruction efficiency [34].

The corresponding upper limit at 90% confidence level on the partial BF, including all uncertainties, is 1.4×10^{-3} for $M(X_{s\bar{s}}) \leq 2.4 \text{ GeV}/c^2$. If $SU(3)$ symmetry holds, then the BFs of $B \rightarrow \eta'X_s$ and $B_s^0 \rightarrow \eta'X_{s\bar{s}}$ would be equivalent and their ratio, $\mathcal{R}(\eta') = \mathcal{B}(B_s^0 \rightarrow \eta'X_{s\bar{s}})/\mathcal{B}(B \rightarrow \eta'X_s)$ would be close to 1 [17]. The measured BF for the decay $B \rightarrow \eta'X_s$ is $[3.9 \pm 0.8 \text{ (stat.)} \pm 0.5 \text{ (syst.)} \pm 0.8 \text{ (model)}] \times 10^{-4}$ [4]. Using this and the weighted average BF given previously for $B_s^0 \rightarrow \eta'X_{s\bar{s}}$, $\mathcal{R}(\eta')$ is approximately -0.2

TABLE II. Results for the $B_s^0 \rightarrow \eta'K^\pm K_S^0 + n\pi$ submodes, from the $121.4 \text{ fb}^{-1} \Upsilon(5S)$ data set; rows with dashes indicate bins where no events, background or signal, were found; the table contains the $M(X_{s\bar{s}})$ bin in units of GeV/c^2 , corrected reconstruction efficiency (ϵ'), number of fitted signal events N_{sig} , and \mathcal{B} , the central value of the partial BF.

$M(X_{s\bar{s}})$	$\epsilon'(\%)$	N_{sig}	$\mathcal{B}(B_s^0 \rightarrow \eta'X_{s\bar{s}}) (10^{-4})$
1.0 - 1.2	0.02 ± 0.006	0.0	-
1.2 - 1.4	0.2 ± 0.02	$0.3^{+1.4}_{-0.8}$	$0.5^{+2.5}_{-1.5} \text{ (stat.) } ^{+0.1}_{-0.04} \text{ (syst.)}$
1.4 - 1.6	0.9 ± 0.04	$2.0^{+3.0}_{-2.2}$	$1.0^{+1.4}_{-1.1} \text{ (stat.) } ^{+0.1}_{-0.07} \text{ (syst.)}$
1.6 - 1.8	0.6 ± 0.04	$1.2^{+3.3}_{-2.6}$	$0.8^{+2.1}_{-1.6} \text{ (stat.) } ^{+0.1}_{-0.1} \text{ (syst.)}$
1.8 - 2.0	0.4 ± 0.03	$4.8^{+4.2}_{-3.4}$	$4.4^{+3.9}_{-3.1} \text{ (stat.) } ^{+0.9}_{-0.7} \text{ (syst.)}$
2.0 - 2.2	0.4 ± 0.03	$-2.4^{+3.9}_{-3.2}$	$-2.8^{+4.6}_{-3.8} \text{ (stat.) } ^{+0.9}_{-0.7} \text{ (syst.)}$
2.2 - 2.4	0.2 ± 0.02	$-1.1^{+3.6}_{-2.9}$	$-2.6^{+8.9}_{-7.1} \text{ (stat.) } ^{+0.2}_{-1.9} \text{ (syst.)}$

$\pm 2.1 \text{ (stat.)} \pm 0.2 \text{ (syst.) } ^{+0.8}_{-1.5} \text{ (FM)} \pm 0.03 (N_{B_s^{0(*)}\bar{B}_s^{0(*)}})$. Applying the same method as used to calculate the upper limit on $\mathcal{B}(B_s^0 \rightarrow \eta'X_{s\bar{s}})$, the 90% confidence level upper limit on $\mathcal{R}(\eta')$ is 3.5.

As a byproduct of the preceding measurement, we searched for the decay $B_s^0 \rightarrow \eta'\phi$, with $\phi \rightarrow K^+K^-$. This decay was searched for in the $X_{s\bar{s}}$ mass subrange $M(X_{s\bar{s}}) \in [1.006, 1.03] \text{ GeV}/c^2$ ($\pm 3\sigma$ window). From MC simulations, the reconstruction efficiency is determined to be $7.90 \pm 0.03\%$. No statistically significant signal is found and the upper limit at 90% confidence level is determined to be 3.6×10^{-5} . The result from fitting is shown in Fig. 4. LHCb determines the upper limit at 90% confidence level to be 8.2×10^{-7} [35].

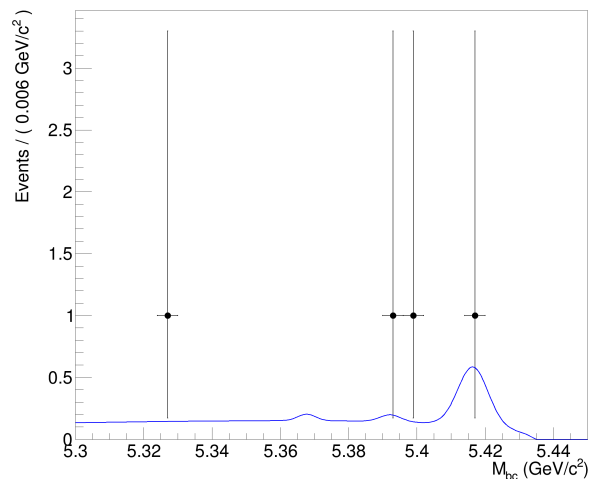


FIG. 4. $B_s^0 \rightarrow \phi(\rightarrow K^+K^-)\eta'$ decay results for $M(X_{s\bar{s}}) \in \pm 3\sigma \phi$ mass range

To conclude, we set an upper limit on the partial BF for the decay $B_s^0 \rightarrow \eta'X_{s\bar{s}}$, for $M(X_{s\bar{s}}) \leq 2.4 \text{ GeV}/c^2$. Including all uncertainties, the upper limit at 90% confidence level is determined to be 1.4×10^{-3} . This is the

first result for the decay $B_s^0 \rightarrow \eta' X_{s\bar{s}}$. Future measurements may help elucidate $SU(3)$ symmetries and enhance the understanding of different penguin contributions to the amplitude of $b \rightarrow sg$ decays. This and future analyses should also help to motivate further studies, both experimental and theoretical, of inclusive B_s^0 processes as there is a dearth of research of the B_s^0 relative to B_d^0 and B_u^\pm .

ACKNOWLEDGMENTS

We thank the KEKB group for excellent operation of the accelerator; the KEK cryogenics group for efficient solenoid operations; and the KEK computer group, the NII, and PNNL/EMSL for valuable computing and SINET5 network support. We acknowledge support from MEXT, JSPS and Nagoya's TLPRC (Japan); ARC (Australia); FWF (Austria); NSFC and CCEPP (China); MSMT (Czechia); CZF, DFG, EXC153, and VS (Germany); DST (India); INFN (Italy); MOE, MSIP, NRF, RSRI, FLRFAS project, GSDC of KISTI and KREONET/GLORIAD (Korea); MNiSW and NCN (Poland); MSHE, Agreement 14.W03.31.0026 (Russia); University of Tabuk (Saudi Arabia); ARRS (Slovenia); IKERBASQUE (Spain); SNSF (Switzerland); MOE and MOST (Taiwan); and DOE and NSF (USA).

Appendix: Discussion of Systematic Uncertainties

The upper limits at 90% confidence level up to a given $X_{s\bar{s}}$ mass bin are given in Table III.

TABLE III. $\mathcal{B}_{UL}^{90\%} \leq M(X_{s\bar{s}})$ 90% upper limits. Upper limit per bin corresponds to the upper limit up to and including that bin in units of $M(X_{s\bar{s}})$.

$M(X_{s\bar{s}})$	$\mathcal{B}(B_s^0 \rightarrow \eta' X_{s\bar{s}}) (10^{-4})$	$\mathcal{B}_{UL}^{90\%} (10^{-4})$
1.2	0.05 ± 0.3 (stat.) $^{+0.01}_{-0.01}$ (syst.)	0.4
1.4	0.08 ± 0.4 (stat.) $^{+0.10}_{-0.04}$ (syst.)	0.7
1.6	0.6 ± 1.0 (stat.) $^{+0.2}_{-0.1}$ (syst.)	1.9
1.8	1.1 ± 1.5 (stat.) $^{+0.3}_{-0.3}$ (syst.)	3.1
2.0	3.8 ± 2.7 (stat.) $^{+1.4}_{-1.3}$ (syst.)	7.6
2.2	3.4 ± 4.8 (stat.) $^{+2.2}_{-1.8}$ (syst.)	11.1
2.4	-0.7 ± 8.1 (stat.) $^{+3.1}_{-6.0}$ (syst.)	13.8

Additive systematic uncertainties are from the PDF parameterization and fit bias. The parameters of the Gaussian signal PDF are allowed to float within their 1σ errors (determined from the $B_s^0 \rightarrow D_s^- \rho^+$ control fit to the $\Upsilon(5S)$ data) and the $\Upsilon(5S)$ data are refitted for the signal yield. The difference in signal yield between the fixed and floated parameterization is taken as the PDF uncertainty. The same is done for the background ARGUS PDF.

The fit bias uncertainty is determined by generating and fitting 5000 MC pseudoexperiments for several assumptions of the branching fraction. This is done using RooStats [36]. The number of fitted signal events versus the number of generated signal events is fitted with a first-order polynomial and the offset from zero of the fit along the y-axis is taken as the uncertainty due to fit bias. The fit bias uncertainty is less than one event. The PDF and fit bias uncertainties are added in quadrature for a total additive systematic uncertainty. This is quoted as the statistical error in Tables I and II in the main report. For $B_s^0 \rightarrow \eta' K^\pm K_S^0 + n\pi$, an uncertainty of 1.1 (26% of the fitted, positive statistical uncertainty) and 1.3 (34%) events are obtained in $X_{s\bar{s}}$ mass bins 1.8 - 2.0 GeV/ c^2 and 2.0 - 2.2 GeV/ c^2 , respectively. All others had uncertainties of less than one event. For $B_s^0 \rightarrow \eta' K^+ K^- + n\pi$, the 1.6 - 1.8 GeV/ c^2 , 1.8 - 2.0 GeV/ c^2 , 2.0 - 2.2 GeV/ c^2 , and 2.2 - 2.4 GeV/ c^2 bins have uncertainties of 1.0 (55%), 1.2 (54%), 3.1 (156%), and 3.0 (132%) events, respectively. All other mass bins each have an uncertainty of less than one event. Additive systematic uncertainties are added in quadrature with the asymmetric fit errors on the signal yield.

Multiplicative systematic uncertainties due to the fragmentation model (FM) of $X_{s\bar{s}}$ by PYTHIA 6 are obtained by an alternate group of JETSET parameters - PARJ(1, 2, 3, 4, 11, 12, 13, 25, 26), which are varied together away from the Belle default to reduce and enhance the (uncorrected) reconstruction efficiency [23]. The uncertainty is

determined from the fractional change in efficiency with respect to the Belle default parameters. This includes the effect of the change in the proportion of unreconstructed modes. If no increase or decrease in efficiency is found then an uncertainty of zero is assigned. Values for the FM uncertainty, per $X_{s\bar{s}}$ mass bin, can be seen in Tables IV and V.

TABLE IV. Summary of FM multiplicative systematic uncertainties for $B_s^0 \rightarrow \eta' K^+ K^- + n\pi$

$M(X_{s\bar{s}})$	FM (%)
1.0 - 1.2	$^{+0.4}_{-5.9}$
1.2 - 1.4	$^{+6.4}_{-2.8}$
1.4 - 1.6	$^{+8.0}_{-8.3}$
1.6 - 1.8	$^{+14.7}_{-35.3}$
1.8 - 2.0	$^{+21.1}_{-33.6}$
2.0 - 2.2	$^{+28.7}_{-37.4}$
2.2 - 2.4	$^{+23.7}_{-58.2}$

TABLE V. Summary of FM multiplicative systematic uncertainties for $B_s^0 \rightarrow \eta' K^\pm K_S^0 + n\pi$

$M(X_{s\bar{s}})$	FM (%)
1.0 - 1.2	$^{+23.7}_{-0.0}$
1.2 - 1.4	$^{+18.3}_{-2.3}$
1.4 - 1.6	$^{+6.6}_{-0.0}$
1.6 - 1.8	$^{+12.5}_{-10.5}$
1.8 - 2.0	$^{+20.2}_{-14.4}$
2.0 - 2.2	$^{+30.7}_{-23.2}$
2.2 - 2.4	$^{+0.0}_{-74.5}$

From the signal MC that is generated and used to determine signal reconstruction efficiency, the proportion of unreconstructed modes is determined by searching in the generated signal MC for modes that contain an $X_{s\bar{s}}$ decay submode but fall outside the criteria for a reconstructed submode, i.e. submodes that contain more than one π^0 , modes with a K_L^0 , or modes with more than six daughter particles (excluding the η'). The proportion of unreconstructed events, defined as $N_{UR}/(N_{UR} + N_R)$, where N_{UR} is the number of generated events from unreconstructed signal modes in signal MC, and N_R is the number of generated events from reconstructed modes. For $B_s^0 \rightarrow \eta' K^+ K^- + n\pi$, 1.1% of events are unreconstructed in the 1.4-1.6 GeV/ c^2 bin, increasing monotonically to 14.5% in the 2.2-2.4 GeV/ c^2 bin. For $B_s^0 \rightarrow \eta' K^\pm K_S^0 + n\pi$ modes, as they are only reconstructed as $B_s^0 \rightarrow \eta' K^\pm K_S^0 + n\pi$, there is a corresponding class of modes that involve a K_L^0 instead of a K_S^0 . This causes the proportion of generated signal events to be higher. In the 1.0-1.2 GeV/ c^2 bin, 48.1% of reconstructable events are unreconstructed, due to unreconstructed K_L^0 modes. This increases monotonically to

59.7% in the 2.2-2.4 GeV/ c^2 bin, of which 84% is due to unreconstructed K_L^0 modes. Using the same signal MC, it is also found that the signal cross-feed efficiency is less than 0.05% in each $X_{s\bar{s}}$ mass bin and is included in the multiplicative systematic uncertainties.

The $B_s^0 \rightarrow D_s^- \rho^+$ control sample is used to determine the systematic uncertainty with respect to the neural network (NN) selection. This uncertainty is obtained by determining the signal yield with and without the neural network selection in both MC and data. The double ratio of these results is determined and its absolute difference from unity is used as the systematic uncertainty. This gives an uncertainty of 6.5% for $B_s^0 \rightarrow \eta' K^+ K^- + n\pi$ and 2.1% for $B_s^0 \rightarrow \eta' K^\pm K_S^0 + n\pi$. The control sample $B_s^0 \rightarrow D_s \rho$ is also used to obtain the uncertainty for best candidate selection (BCS). The uncertainty is obtained by determining the signal yield with and without best candidate selection in both MC and data. The double ratio of these results is determined and its absolute difference from unity is used as the systematic uncertainty. This gives an uncertainty of 1.0% for $B_s^0 \rightarrow \eta' K^+ K^- + n\pi$ and 4.4% for $B_s^0 \rightarrow \eta' K^\pm K_S^0 + n\pi$, using the neural network selection of these associated classes of signal modes. The uncertainty for the reconstruction of $\eta \rightarrow \gamma\gamma$ and $\pi^0 \rightarrow \gamma\gamma$ is 3.0% [37].

The uncertainty on charged track reconstruction is 0.35% per track [38]. The uncertainty on the efficiency to identify charged kaons and pions is a function of their momenta and polar angles. The uncertainty for K^\pm and π^\pm identification is 0.95% and 1.8%, respectively. The K_S^0 reconstruction uncertainty is 1.6% [39]. The total track uncertainty, for each source, per $X_{s\bar{s}}$ mass bin, is obtained by determining the average charged kaon and charged pion multiplicity (M) in signal MC and multiplying the uncertainty by that multiplicity, e.g. $M(0.182)$. These uncertainties are added linearly as they are uncertainties of common daughters of a single mother particle (B_s^0) and are thus correlated.

The $\Upsilon(5S)$ production model (PM) uncertainty leads to a fractional change in reconstruction efficiency of $B_s^{0*} \bar{B}_s^{0*}$ S -wave ($L = 0$) states in a $B \rightarrow D_s \pi$ control sample MC, with and without the model in [40], is implemented. The uncertainty is approximately 0.2% for $B_s^0 \rightarrow \eta' K^\pm K^0 + n\pi$ and 1.1% for $B_s^0 \rightarrow \eta' K^\pm K_S^0 + n\pi$. The uncertainty on the subdecay mode branching fractions $\mathcal{B}(\eta \rightarrow \gamma\gamma)$ and $\mathcal{B}(\eta' \rightarrow \eta\pi\pi)$ are 0.2% and 0.7%, respectively [27]. Estimates of individual multiplicative systematic uncertainties can be seen in Table VI. Totals of these uncertainties are determined in individual $X_{s\bar{s}}$ mass bins.

TABLE VI. Summary of multiplicative systematic uncertainties. The uncertainties for particle identification and reconstruction are evaluated per $X_{s\bar{s}}$ mass bin.

Uncertainty Source	Value (%)
π^0 Reconstruction	3.0
K_S^0 Reconstruction	1.6
Charged Track Reconstruction	0.4
K^\pm ID	0.95
π^\pm ID	1.3
$\Upsilon(5S)$ PM ($B_s^0 \rightarrow \eta' K^+ K^- + n\pi$)	0.2
$\Upsilon(5S)$ PM ($B_s^0 \rightarrow \eta' K^\pm K_S^0 + n\pi$)	1.1
η Reconstruction	3.0
NN Selection ($B_s^0 \rightarrow \eta' K^+ K^- + n\pi$)	6.5
NN Selection ($B_s^0 \rightarrow \eta' K^\pm K_S^0 + n\pi$)	2.1
BCS ($B_s^0 \rightarrow \eta' K^+ K^- + n\pi$)	1.0
BCS ($B_s^0 \rightarrow \eta' K^\pm K_S^0 + n\pi$)	4.4
$\mathcal{B}(\eta \rightarrow \gamma\gamma)$	0.2
$\mathcal{B}(\eta' \rightarrow \eta\pi\pi)$	0.7
$N_{B_s^{0(*)} \bar{B}_s^{0(*)}}$	18.3

-
- [1] A. J. Bevan *et al.*, Eur. Phys. J. C **74**, 3026 (2014).
- [2] T. E. Browder *et al.* (CLEO Collaboration), Phys. Rev. Lett. **81**, 1786 (1998).
- [3] G. Bonvicini *et al.* (CLEO Collaboration), Phys. Rev. D **68**, 011101 (2003).
- [4] B. Aubert *et al.* (BABAR Collaboration), Phys. Rev. Lett. **93**, 061801 (2004).
- [5] K. Nishimura *et al.* (Belle Collaboration), Phys. Rev. Lett. **105**, 191803 (2010).
- [6] K. Ottnad and C. Urbach (ETM Collaboration), Phys. Rev. D **97**, 054508 (2018).
- [7] A. Datta, X.-G. He, and S. Pakvasa, Phys. Lett. B **419**, 369 (1998).
- [8] D. Atwood and A. Soni, Phys. Lett. B **405**, 150 (1997).
- [9] A. L. Kagan and A. Petrov, (1997), arXiv:hep-ph/9707354 [hep-ph].
- [10] H. Fritzsch, Phys. Lett. B **415**, 83 (1997).
- [11] W.-S. Hou and B. Tseng, Phys. Rev. Lett. **80**, 434 (1998).
- [12] A. Ali and A. Y. Parkhomenko, (2001), arXiv:hep-ph/0112048 [hep-ph].
- [13] X.-G. He and G.-L. Lin, Phys. Lett. B **454**, 123 (1999).
- [14] E. Kou, Phys. Rev. D **63**, 054027 (2001).
- [15] S. Dubey, *Search for the decay $B_s^0 \rightarrow \eta' X_{s\bar{s}}$ Using a Semi-Inclusive Method at the Belle Experiment*, Ph.D. thesis, University of Hawaii at Manoa (2020), unpublished.
- [16] T. Abe *et al.*, Prog. Theor. Exp. Phys. **2013**, 03A001 (2013).
- [17] A. Datta (University of Mississippi), private communication (2020).
- [18] J. Brodzicka *et al.*, Prog. Theor. Exp. Phys. **2012**, 04D001 (2012).
- [19] S. Esen *et al.* (Belle Collaboration), Phys. Rev. D **87**, 031101 (2013).
- [20] D. J. Lange, Nucl. Instrum. and Meth. A **462**, 152 (2001).
- [21] R. Brun *et al.*, GEANT 3.21, CERN Report DD/EE/84-1 (1984).
- [22] E. Barberio, B. van Eijk, and Z. Was, Comp. Phys. Commun. **66**, 115 (1991).
- [23] T. Sjostrand, S. Mrenna, and P. Skands, JHEP **2006** (2006), 026.
- [24] H. Hirano *et al.*, Nucl. Instrum. and Meth. A **455**, 294 (2000).
- [25] T. Iijima *et al.*, Nucl. Instrum. and Meth. A **453**, 321 (2000).
- [26] H. Kichimi *et al.*, Nucl. Instrum. and Meth. A **453**, 315 (2000).
- [27] P. Zyla *et al.* (Particle Data Group), Prog. Theor. Exp. Phys. **2020**, 083C01 (2020).
- [28] G. C. Fox and S. Wolfram, Phys. Rev. Lett. **41**, 1581 (1978).
- [29] M. Feindt and U. Kerzel, Nucl. Instrum. and Meth. A **559**, 190 (2006).
- [30] S. H. Lee *et al.* (Belle Collaboration), Phys. Rev. Lett. **91**, 261801 (2003).
- [31] H. Albrecht *et al.* (ARGUS Collaboration), Phys. Lett. B **241**, 278 (1990).
- [32] The number of unreconstructed modes is discussed in the the appendix.
- [33] A discussion of the uncertainties is given in the accompanying appendix.
- [34] Estimates of the FM uncertainty are given in the appendix.
- [35] R. Aaij *et al.* (LHCb Collaboration), JHEP **1705**, 158 (2017).
- [36] L. Moneta *et al.*, (2010), arXiv:1009.1003 [physics.data-an].
- [37] B. Pal *et al.* (Belle Collaboration), Phys. Rev. D **92**, 011101 (2015).
- [38] S. Ryu *et al.* (Belle Collaboration), Phys. Rev. D **89**, 072009 (2014).
- [39] N. Dash *et al.* (Belle Collaboration), Phys. Rev. Lett. **119**, 171801 (2017).
- [40] A. Abdesselam *et al.*, (2016), arXiv:1609.08749.